Identification of Motor Control Objectives in Human Locomotion via Multi-Objective Inverse Optimal Control

Matilde Tomasi
Ph.D. Student
Department of Civil and Industrial Engineering
Università di Pisa
56122 Pisa, Italy
Email: matilde.tomasi@phd.unipi.it

Alessio Artoni*
Associate Professor
Department of Civil and Industrial Engineering
Università di Pisa
56122 Pisa, Italy
Email: alessio.artoni@unipi.it

ABSTRACT

Predictive simulations of human motion are a precious resource for a deeper understanding of the motor control policies encoded by the central nervous system. They also have profound implications for the design and control of assistive and rehabilitation devices, for ergonomics, as well as for surgical planning. However, the potential of state-of-the-art predictive approaches is not fully realized yet, making it difficult to draw convincing conclusions about the actual optimality principles underlying human walking. In the present study we propose a novel formulation of a bilevel, inverse optimal control strategy based on a full-body three-dimensional neuromusculoskeletal model. In the lower level, prediction of walking is formulated as a principled multi-objective optimal control problem based on a weighted Chebyshev metric, whereas the contributions of candidate control objectives are systematically and efficiently identified in the upper level. Our framework has proved to be effective in determining the contributions of the selected objectives and in reproducing salient features of human locomotion. Nonetheless, some deviations from the experimental kinematic and kinetic trajectories have emerged, suggesting directions for future research. The proposed framework can serve as an inverse optimal control platform for testing multiple optimality criteria, with the ultimate goal of learning the control objectives that best explain observed human motion.[1]

*Address all correspondence to this author
[1] A preliminary version of this paper was presented at the ASME IDETC/CIE 2022 Conference as Paper No. DETC2022-89536

1 INTRODUCTION

Human walking is the result of a long and complex evolution in which locomotion-generator neural circuits and the musculoskeletal system progressively modified with respect to quadrupeds. Its apparent simplicity, but real complexity, has always aroused considerable interest in the biomechanics community, with Leonardo Da Vinci being one of the pioneers in making scientific observations about human locomotion [1]. Modern techniques of motion capture/analysis combined with neuromusculoskeletal (NMS) models are an important instrument for developing a deeper understanding of the principles underlying human movement. Such tools are typically used to investigate the internal workings of the NMS system, e.g. to estimate muscle forces [2] and joint loads [3]. Recently, strategies based on NMS modeling and optimal control (planning) have begun to show their potential as *synthesis* tools for model-based *prediction* of walking [4, 5, 6]. The availability of *validated*, predictive simulations would promote important investigations: in particular, they would advance the comprehension of the control policy adopted by the central nervous system when we walk, shedding light on internal mechanisms that are not yet fully understood, such as muscle recruitment criteria. Also, such predictive simulations would provide valuable information for planning surgeries and rehabilitation treatments, for ergonomics, and for the design and control of assistive devices.

On the basis of experimental evidence, several studies suggest optimality in the way we walk, as well as concurrence of multiple optimality criteria (e.g., energy expenditure, mechanical power, muscle activity, etc.) [7, 8, 9, 10]. Assuming that such optimality really carries a mathematical connotation and optimality models can be adopted (see also the interesting discussion in [11] about evolutionary adaptation), researchers have been formulating model-based optimal control problems (OCPs) to predict human locomotion both in healthy and pathological subjects. For example, optimal control techniques have recently been used to predict a crutch walking pattern [12] and the crouch gait of children with cerebral palsy [13, 14], or to help design prostheses and exoskeletons [15, 16, 17]. Outside the clinical context, predictive simulations can aid athletes in optimizing their performance and reducing the risk of injury [18]. Although the potential of these techniques is clear, it has not been fully realized yet.

State-of-the-art predictive simulations mainly differ in two respects: the level of complexity of the NMS model, and the objective function(s) (Lagrange term) of the OCP. Obviously, physical fidelity (realism) of the model is crucial to obtaining valid results, but sophisticated models are often computationally expensive or even intractable. To mitigate computational cost, many researchers have employed NMS models with relatively few degrees of freedom (DOFs) and simple muscles (e.g., [19, 20, 21, 22]). Also, the arms are not modeled explicitly in most works: their inertial properties are simply lumped with those of the head and torso.

Although the reasons why arms swing in opposition to the legs are still controversial [23], excluding them from a model reduces its physical fidelity: indeed, it has been shown that arm swing helps minimize energy consumption and optimize stability by reducing the vertical component of the ground reaction moment [24]. The formulation of a dynamic optimization problem of human walking by Anderson and Pandy in 2001 [25] was most likely the first of its kind: their three-dimensional NMS model had 23 DOFs and 54 musculotendon actuators (but the arms were lumped with the head and torso into a single rigid body), and the solution required almost fourteen months of CPU time in those days. The modern, advanced OCP implementation by Falisse et al. in 2019 [4] includes a model with 29 DOFs and 92 musculotendon actuators, arms with 8 ideal torque actuators, and a CPU time of about 20 minutes on a single-core laptop computer (2.9 GHz processor).

With regard to objective functions, which are in fact motor control objectives (the two terms will be used interchangeably), several predictive simulations have been formulated as single-objective OCPs: as corroborated by experimental evidence whereby humans walk at speeds which correspond to minimum energy consumption [9, 26], many authors have suggested minimizing some form of energy to predict walking and running [25, 27, 28, 29]. Nonetheless, other criteria revolving around muscle activations also seem to play an important role in synthesizing features of bipedal locomotion. Among these, fatigue-like and effort-like criteria have often been used as additional objective functions [19, 30]. Also optimization of smoothness, expressed for example as the time-derivative of muscle activations or of joint torques, has been found to drive predictive simulations towards better solutions [10, 31]. All these aspects suggest that human locomotion could involve multiple optimality principles. However, inferring such control objectives and their contributions is still an open problem: recently, it has been tackled by means of promising *bilevel*, *inverse OCP* formulations [21, 22, 32, 33].

Despite the above-mentioned progress in this field, several improvements are needed, as evidenced by the marked discrepancies between the trajectories of predicted and measured biomechanical variables. In this paper we set out to deal with a major limitation that, to the best of our knowledge, has never been exposed but concerns the totality of the works in this research domain, both in forward and inverse OCPs of human movement: the way in which concurrent control objectives are handled. Multiple objectives are typically aggregated into a single objective function through a simple linear combination of them (a weighted sum) [34], but this approach has two important drawbacks, as will become apparent in the next sections. First, potentially good solutions may be very easily missed. Second, the values of the weights of the objectives may be deceptive or even grossly misleading when it comes to the interpretation of their relative

importance/contributions. Our method is aimed at overcoming said limitations while retaining the simplicity and expressiveness of weights, and it is applied to the domain of bilevel inverse optimal control for the identification of control objectives in predictive simulations of unimpaired human walking. The formulation we propose leverages fundamental concepts from multi-objective optimization to explore the entire Pareto-optimal front of pre-selected, candidate control objectives, and it attempts to do so while maximizing computational efficiency.

2 METHODS

2.1 Prediction of walking as a model-based OCP

As discussed in the Introduction, many predictive simulations of human walking have been framed as model-based forward OCPs that include multiple control objectives and can be compactly expressed as

$$\min_{(\mathbf{x}(t),\mathbf{u}(t))\in\Omega} \Big(J\big(\mathbf{x}(t),\mathbf{u}(t);\mathbf{w}\big) = \sum_{i=1}^{m} w_i J_i\big(\mathbf{x}(t),\mathbf{u}(t)\big) \Big) \tag{1a}$$

$$\Omega = \big\{ \big(\mathbf{x}(t),\mathbf{u}(t)\big) : \dot{\mathbf{x}} = \mathbf{f}\big(\mathbf{x},\mathbf{u}\big),\ \mathbf{h}\big(\mathbf{x},\mathbf{u}\big) \geq \mathbf{0} \big\} \tag{1b}$$

where, given a set of weights $\mathbf{w} = (w_1,\ldots,w_m)$ to linearly combine the m pre-selected objective function(al)s $\mathbf{J}\big(\mathbf{x}(t),\mathbf{u}(t)\big) = \big(J_i\big(\mathbf{x}(t),\mathbf{u}(t)\big),\ i = 1,\ldots,m\big)$ into the single objective $J\big(\mathbf{x}(t),\mathbf{u}(t);\mathbf{w}\big)$, the goal is to obtain the trajectories of states, $\mathbf{x}(t)$, and controls, $\mathbf{u}(t)$, that minimize J subject to the constraints defining the feasible region Ω, i.e. the first-order dynamic constraints of the NMS model and other algebraic path constraints $\mathbf{h}$ (initial and endpoint conditions can be included here, as well as bound constraints on the optimization variables). The continuous problem (1) is typically discretized using multiple shooting or a direct collocation method, and the resulting nonlinear optimization problem is solved [35].

The choice of the objective functions and their weights is obviously critical to the results of predictive simulations. Typically, the m candidate objectives $\mathbf{J}$ are pre-selected, whereas their weights $\mathbf{w}$ are adjusted so as to qualitatively obtain a human-like gait [4] or to reduce the deviations between the predicted trajectories of some states/controls and their experimental counterparts, as done in [36]. This process of manually tuning the weights is mostly based on trial-and-error or on preset weighting schemes, thus it is usually slow and certainly prone to sub-optimality. In order to improve weight selection and to make it a less subjective procedure, approaches based on inverse optimal control have recently received attention.

The predictive framework proposed in this study is based on the three-dimensional NMS model developed in [4] through OpenSim [37]. Its 29 DOFs include 3 rotations and 3 translations for the pelvis with respect to the ground, 3 rotations at each hip, 1 rotation at each knee, 2 rotations at each ankle, 3 rotations at the lumbar joint, 3 rotations at each shoulder and 1 rotation at each elbow. Forty-three Hill-type musculotendon units [38] actuate each leg and 6 actuate the lumbar joint, whereas each arm is provided with 4 ideal torque actuators. Foot-ground contact is modeled by 6 compliant Hunt-Crossley spheres (a penalty-based contact model) per foot. The anthropometry of the model was scaled so as to match a specific subject (healthy female, 35 years; mass: 62 kg; height: 1.70 m) whose experimental gait data were available [4]. We solve predictive OCPs (Eqn. (1)) drawing on the computational framework developed and made available by Falisse et al. [4] in a MATLAB-CasADi [39] environment, which we modified to meet the goals of our investigation. The continuous OCP is discretized into 50 nodes per half gait cycle (gait symmetry and periodicity are imposed as path constraints) according to a direct collocation scheme. The resulting nonlinear optimization problem is solved by the interior-point solver IPOPT [40] exploiting the problem's sparsity. Derivatives required by the solver are calculated efficiently and accurately (to working precision) by CasADi through algorithmic differentiation. For a thorough description of the NMS model and computational framework, the reader is referred to [4] and its supplementary material, where all the states $\mathbf{x}$ (e.g., joint angles, joint velocities, etc.) and controls $\mathbf{u}$ (e.g., joint accelerations, arm excitations, etc.) as well as the problem's constraints are fully detailed.

2.2 Identification of control objective weights as an inverse OCP

Inverse optimal control is aimed at learning the control objectives that best explain demonstrated optimal behavior. With a pre-selected set of candidate objectives, this amounts to determining the weights $\mathbf{w}$ in Eqn. (1) avoiding manual guess-and-tune procedures. In some studies, richer, non-parametric objective function models based on Gaussian processes, neural networks, radial basis functions, etc. are employed, especially in works belonging to the closely related field of machine learning (where inverse optimal control is called inverse reinforcement learning): the intrinsic disadvantage of this approach is that interpretability of the objectives is lost, and also well-engineered regularization terms are often required (cf. the recent review [34]). In our case, it is quite difficult to know if we fundamentally need more or different objective functions that better encode the control policy underlying human walking, but we certainly need to pursue the "correct" combination of the ones we have selected. To this end, inverse OCPs formulated as bilevel optimization problems have been proposed. Bilevel weight identification is based on forming an upper-level

optimization around a lower-level OCP: at each upper-level iteration, the lower-level OCP (i.e., Eqn. (1)) is solved with a specific set of weights and the results are rated relative to the experimental gait data, then iterations proceed until suitable termination conditions are satisfied. In more mathematical terms, such parameter estimation problem can be expressed as follows:

$$\min_{\mathbf{w}} \quad d\big(\mathbf{w}; \bar{\mathbf{x}}(t), \bar{\mathbf{u}}(t)\big) \tag{2a}$$

$$\text{s. t.} \quad \big(\bar{\mathbf{x}}(t), \bar{\mathbf{u}}(t)\big) = \underset{(\mathbf{x}(t),\mathbf{u}(t))\in\Omega}{\operatorname{argmin}} J\big(\mathbf{x}(t), \mathbf{u}(t); \mathbf{w}\big) \tag{2b}$$

where the upper-level objective function d in Eqn. (2a) is a measure of the deviations between the experimentally available gait data and the corresponding states $\bar{\mathbf{x}}(t)$ and controls $\bar{\mathbf{u}}(t)$ predicted in the nested lower-level OCP (Eqn. (2b), an instance of the problem expressed by Eqn. (1)).

2.3 Selection of candidate control objectives

The control objectives J_i in Eqn. (1) are usually selected from a set of function models including energy features (e.g., metabolic energy and total work), kinematic features (velocity, acceleration, jerk), dynamic features (torque, torque variation), and other physiological criteria that are assumed to capture the nature of the considered motor task [34].

The same five control objectives as those in [4] were adopted here to facilitate comparisons. They are expressed as continuous-time integral costs and, after discretization, computed by numerical quadrature. Explicit dependence on $\big(\mathbf{x}(t), \mathbf{u}(t)\big)$ will be omitted hereafter for brevity.

1. Squared 2-norm of the vector $\mathbf{a}$ of all muscle activations ($\mathbf{a} \subset \mathbf{x}$):

$$J_1 = \frac{1}{D} \int_0^{t_f} \|\mathbf{a}\|_2^2 \, \mathrm{d}t,$$

where D is the total forward distance traveled by the pelvis and t_f is the final time (both are parameters of the OCP, to be determined).

2. Squared 2-norm of the vector $\mathbf{e}_a$ of the excitations of the arms' ideal torque actuators ($\mathbf{e}_a \subset \mathbf{u}$):

$$J_2 = \frac{1}{D} \int_0^{t_f} \|\mathbf{e}_a\|_2^2 \, \mathrm{d}t$$

3. Squared 2-norm of the vector $\dot{\mathbf{E}}$ of the metabolic energy rates of all muscles, computed according to the model described in [41]:

$$J_3 = \frac{1}{D} \int_0^{t_f} \|\dot{\mathbf{E}}\|_2^2 \, \mathrm{d}t$$

4. Squared 2-norm of the vector $\ddot{\mathbf{q}}_{\mathrm{lt}}$ of the joint accelerations of the lower limbs and trunk, as a measure of motion smoothness ($\ddot{\mathbf{q}}_{\mathrm{lt}} \subset \mathbf{u}$):

$$J_4 = \frac{1}{D} \int_0^{t_f} \|\ddot{\mathbf{q}}_{\mathrm{lt}}\|_2^2 \, \mathrm{d}t$$

5. Squared 2-norm of the vector $\mathbf{T}_p$ of the passive joint torques, representing the actions of ligaments and other passive structures (this term was also used in [25] to penalize joint overextension):

$$J_5 = \frac{1}{D} \int_0^{t_f} \|\mathbf{T}_p\|_2^2 \, \mathrm{d}t$$

2.4 Aggregation of the candidate control objectives

The control objectives J_i in the lower-level OCP are typically aggregated into a scalar-valued objective function J by linearly combining them through weights w_i, as explicitly shown in Eqn. (1a). Such a combination is the major common limitation we have observed in published works on forward and inverse OCP formulations for the prediction of human movement. To fully grasp the causes of said limitation, some concepts from multi-objective optimization need to be introduced.

The concurrent objectives J_i can be *conflicting* in general, and this is typically not known a priori. The individual minima of conflicting objectives are independent from each other (i.e., if one objective is

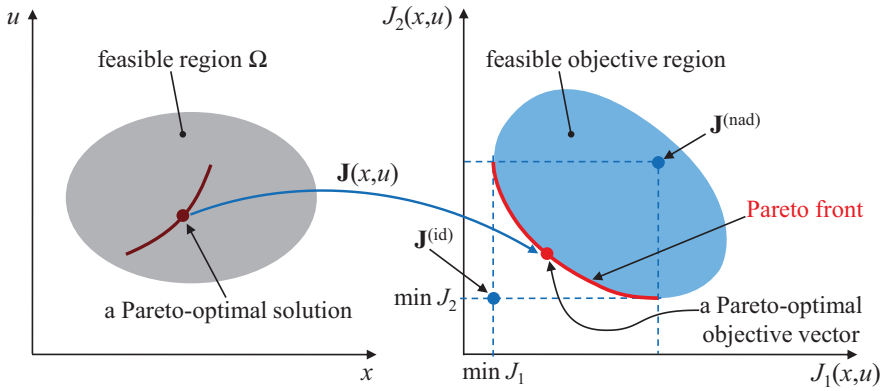

Fig. 1. Graphical representation of a two-variable two-objective convex MOP

minimized, the others are not). Whenever this happens, we are faced with a multi-objective optimization problem (MOP), which can be compactly expressed (for the OCP at hand) as:

$$\min_{(\mathbf{x},\mathbf{u})\in\Omega} \mathbf{J}(\mathbf{x},\mathbf{u}) \tag{3}$$

Please recall that the continuous-time functions $\mathbf{x}(t)$ and $\mathbf{u}(t)$ are discretized into the sequences $(\mathbf{x}_k)_{k=0}^{N}$ and $(\mathbf{u}_k)_{k=0}^{N}$ (here, $N = 50$ in a half gait cycle), which are the effective optimization variables. Simultaneous minimization of the m objectives generally has infinitely many solutions, called Pareto-optimal (or compromise) solutions, whose corresponding objective vectors form the Pareto-optimal (PO) front. For each of these solutions, a further reduction in one of the objectives (satisfying the problem's constraints) necessarily entails an increase in at least another objective. A pictorial representation of an example two-variable two-objective MOP is provided in Fig. 1: the points of the feasible region Ω (left) are mapped by $\mathbf{J}$ to the feasible objective region (right), where the red curve is the PO front. The individual minima of J_1 and J_2 are distinct, thus the two objectives are conflicting.

When objectives and constraints are convex functions, one has a convex MOP, characterized by a convex PO front (as in Fig. 1). However, just one nonconvex objective or constraint function will suffice to obtain a nonconvex MOP, hence a potentially *nonconvex PO front*. Most control objectives and constraint functions in the OCP of human walking are typically nonlinear, which may easily result in a nonconvex front. In real world problems, the PO front is unknown and needs to be explored.

MOPs can be solved through *scalarization*, which converts the vector-valued objective function into a scalar objective function. The best-known scalarization technique is the ubiquitous weighting method,

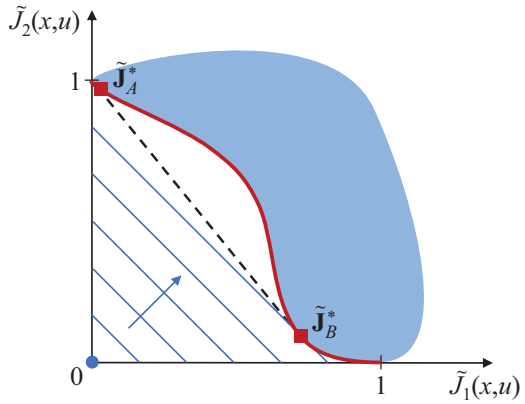

Fig. 2. PO front of a two-objective nonconvex MOP

which is exactly what is done in Eqn. (1a) or (2b): the control objectives are linearly combined through the weights $\mathbf{w}$ and, by minimizing the single objective J with a specific set of weights, one obtains a PO solution and its corresponding PO objective vector (point of the PO front). Please note that *solving the bilevel optimization problem* (2) *amounts to identifying the special set of weights, hence the PO objective vector, that results in the minimum deviation between predicted and experimental gait data*. Multiple control objectives in published works on the prediction of human movement have always been aggregated according to the weighting method [34]. However, despite its ease of implementation and apparent simplicity of interpretation, this method has a number of important limitations, especially in nonconvex MOPs: (i) it cannot obtain solutions in nonconvex regions of the PO front, (ii) weights may be difficult to interpret or entirely misleading, and (iii) evenly distributed weights may not yield evenly distributed PO objective vectors.

Let us delve a little deeper into these aspects with the help of Fig. 2 after highlighting the importance of *normalization* of the objectives. The first step in properly handling the objectives is indeed to *normalize* them over the PO front: normalization yields objectives of the same magnitude and range, which allows to compare them in a mathematically meaningful way. To this end, the ideal objective vector $\mathbf{J}^{(\mathrm{id})}$ and the nadir objective vector $\mathbf{J}^{(\mathrm{nad})}$ should be estimated (see also Fig. 1). These two vectors represent, respectively, the lower and the upper bounds of the PO front. While $\mathbf{J}^{(\mathrm{id})}$ is the result of minimizing the objectives individually, $\mathbf{J}^{(\mathrm{nad})}$ represents their maximum values over the PO front, and it can be approximated using a pay-off table if more than two objectives are present [42]. Each objective J_i should thus be replaced by its normalized "J_i-tilde" version:

$$\tilde{J}_i(\mathbf{x},\mathbf{u}) = \frac{J_i(\mathbf{x},\mathbf{u}) - J_i^{(\mathrm{id})}}{J_i^{(\mathrm{nad})} - J_i^{(\mathrm{id})}}, \tag{4}$$

thus problem (1) can be now recast as

$$\min_{(\mathbf{x},\mathbf{u})\in\Omega} \left(\tilde{J}(\mathbf{x},\mathbf{u};\mathbf{w}) = \sum_{i=1}^{m} w_i \tilde{J}_i(\mathbf{x},\mathbf{u})\right), \quad \sum_{i=1}^{m} w_i = 1 \tag{5}$$

As shown in Fig. 2, any PO objective vector has its components between 0 and 1 after (perfect) normalization (also, $\tilde{\mathbf{J}}^{(\text{id})} = \mathbf{0}$ and $\tilde{\mathbf{J}}^{(\text{nad})} = \mathbf{1}$). Figure 2 shows the weighting method in action on a nonconvex MOP with equal weights $\mathbf{w} = (0.5, 0.5)$: the nonconvex part of the red PO curve is the portion delimited by the PO objective vectors $\tilde{\mathbf{J}}^*_A$ and $\tilde{\mathbf{J}}^*_B$ (points of tangency between the dashed line and the PO front); the contour lines of the scalar objective function $\tilde{J}$ (in Eqn. (5)) are also shown, with its values increasing as one moves away from the origin. By minimizing $\tilde{J}$ subject to the constraints Ω (that is, solving the OCP (5)), one obtains a PO objective vector that can be easily identified: it is the point of tangency between said contour lines and the PO front, almost coincident with point $\tilde{\mathbf{J}}^*_B$ (but not shown in Fig. 2), and quite distant from the logical intuition/interpretation that equal weights should produce a PO objective vector somewhere in the middle of the PO front, ideally halfway between the individual minima of $\tilde{J}_1$ and $\tilde{J}_2$. By changing the weights one generally obtains a different PO objective vector, *but no choice of* $\mathbf{w}$ *can yield any of the PO points in the nonconvex region between* $\tilde{\mathbf{J}}^*_A$ *and* $\tilde{\mathbf{J}}^*_B$*, thus missing many PO solutions*. Furthermore, if the selected weights are such that the corresponding function $\tilde{J}$ has contours inclined as the dashed line through $\tilde{\mathbf{J}}^*_A$ and $\tilde{\mathbf{J}}^*_B$, then $\tilde{J}$ would have two minima (at $\tilde{\mathbf{J}}^*_A$ and $\tilde{\mathbf{J}}^*_B$), and the actual solution would mostly depend on the initial guess: this sort of "jump" can be a source of numerical instability.

How can we overcome these limitations intrinsic to the weighting method? Several multi-objective optimization methods have been developed that improve on the weighting method and can theoretically obtain any PO objective vector of both convex and nonconvex PO fronts (see, e.g., [42]), but our goal is to retain the simplicity and expressiveness of weights to combine our control objectives. To this end, we aggregate the objectives by adopting a special weighted metric, namely the *weighted Chebyshev norm*, thus replacing problem (5) with[2]

$$\min_{(\mathbf{x},\mathbf{u})\in\Omega} \left(\tilde{J}_C(\mathbf{x},\mathbf{u};\mathbf{w}) = \max_{i=1,\ldots,m} w_i \tilde{J}_i(\mathbf{x},\mathbf{u})\right), \quad \sum_{i=1}^{m} w_i = 1 \tag{6}$$

[2]The relationship between the weighted Chebyshev metric and Pareto optimality was first investigated by Bowman in 1976 [43]

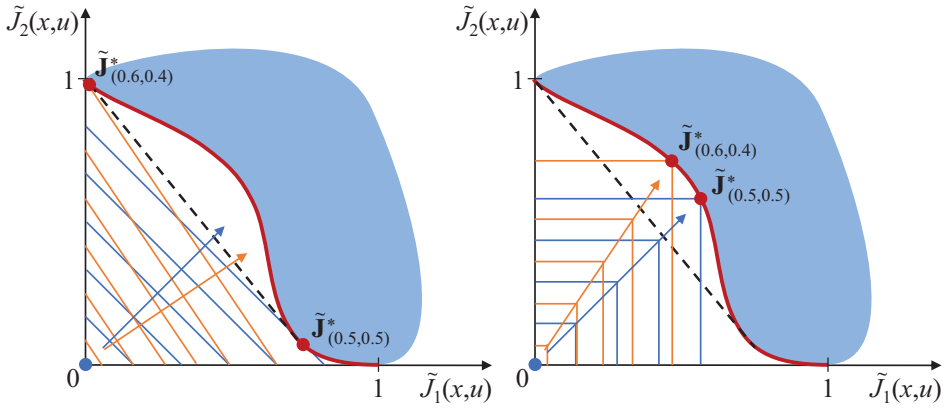

Fig. 3. Weighting method (left) vs. weighted Chebyshev method (right) with weights $(0.5, 0.5)$ and $(0.6, 0.4)$ on a nonconvex MOP

The performances of the weighting method and the weighted Chebyshev method on a nonconvex MOP are contrasted in Fig. 3 using two different sets of weights, $(0.5, 0.5)$ and $(0.6, 0.4)$. Two important aspects deserve attention. First, thanks to the shape of the contour lines of its scalarizing function $\tilde{J}_C$ (featuring "kinks"), the Chebyshev method can obtain any PO objective vector in the nonconvex region of the PO front. Second, the position of such PO objective vectors on the PO front reflect the relative importance implied by their weights (Fig. 3): $\tilde{\mathbf{J}}^*_{(0.5,0.5)}$ is approximately in the middle of the Pareto front with the Chebyshev method, while it is close to the individual minimum of $\tilde{J}_2$ with the weighting method; with the Chebyshev method, $\tilde{\mathbf{J}}^*_{(0.6,0.4)}$ moderately improves on $\tilde{J}_1$ at the expense of $\tilde{J}_2$, as expected and "meant", whereas $\tilde{\mathbf{J}}^*_{(0.6,0.4)}$ obtained by the weighting method is very close to the individual minimum of $\tilde{J}_1$.

Problem (6) is nonsmooth because it includes the $\max$ function, which may cause numerical difficulties when the partial derivatives required to solve the optimization problem are calculated: all objective and constraint functions should be differentiable, especially for the algorithmic differentiation routines implemented in CasADi. With this in mind, we replaced the $\max$ function with its scale-invariant, p-norm approximation (other differentiable reformulations are possible). Recall that, for any vector $\mathbf{v} \in \mathbb{R}^n$, $\|\mathbf{v}\|_p = \max(|v_1|, \ldots, |v_n|)$ as $p \to \infty$. We selected $p = 100$ to obtain a good approximation, thus function $\tilde{J}_C$ becomes:

$$\tilde{J}_{sC}(\mathbf{x}, \mathbf{u}; \mathbf{w}) = \left\| \left(w_1 \tilde{J}_1(\mathbf{x}, \mathbf{u}), \ldots, w_m \tilde{J}_m(\mathbf{x}, \mathbf{u}) \right) \right\|_{100} \tag{7}$$

where subscript sC stands for "smoothed Chebyshev", and absolute values have been removed because our five objectives $(\tilde{J}_1, \ldots, \tilde{J}_5)$ are nonnegative. Graphically, the contour lines of $\tilde{J}_{sC}$ are very close to those

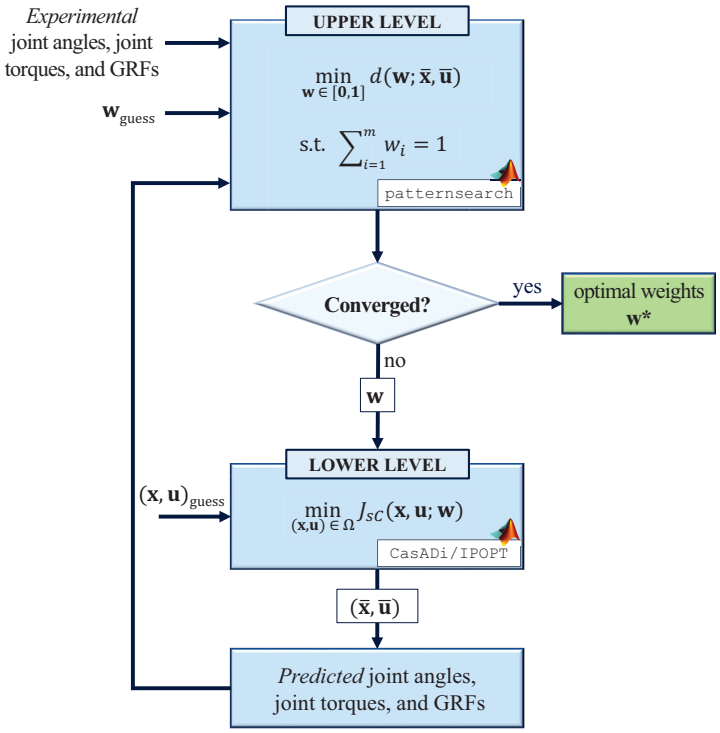

Fig. 4. Flowchart of the proposed bilevel optimization framework.

of $\tilde{J}_C$, but the sharp corners in the latter are replaced by smooth fillets.

2.5 Proposed inverse optimal control formulation

In light of the various aspects discussed thus far, we propose to identify the control objective weights in human locomotion by formulating the following bilevel, inverse OCP (cf. Eqn. (2)), which is also schematically illustrated by the flowchart in Fig. 4:

$$\min_{\mathbf{w}\in[\mathbf{0},\mathbf{1}]} \quad d(\mathbf{w};\bar{\mathbf{x}},\bar{\mathbf{u}}) \tag{8a}$$

$$\text{s. t.} \quad (\bar{\mathbf{x}},\bar{\mathbf{u}}) = \underset{(\mathbf{x},\mathbf{u})\in\Omega}{\operatorname{argmin}} \tilde{J}_{sC}(\mathbf{x},\mathbf{u};\mathbf{w}) \tag{8b}$$

$$\sum_{i=1}^{m} w_i = 1 \tag{8c}$$

where the *deviation* d is obtained by aggregating three scalar indices (d_a, d_g, d_t)[3] that respectively quantify the deviations of predicted joint angles, ground reaction forces, and joint torques from their experimental

[3]The three indices were aggregated using the weighted Chebyshev norm (with equal weights) after their normalization

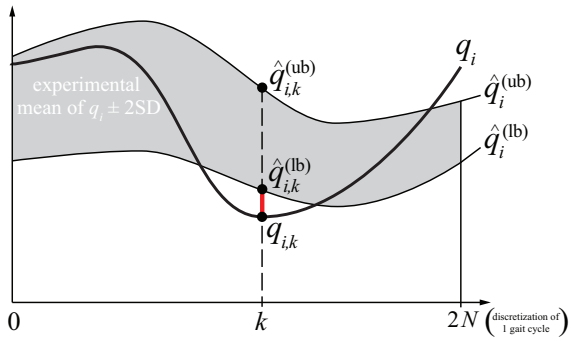

Fig. 5. Quantities used to calculate the deviation index d_a. q_i is the i-th predicted joint angle, $\hat{q}_i^{(\mathrm{ub})}$ is the set of its experimental upper values (mean+2SD), and $\hat{q}_i^{(\mathrm{lb})}$ the set of its experimental lower values (mean−2SD).

counterparts (available for the subject previously described). Figure 5 helps understand how each deviation index was calculated. The basic idea is that each predicted variable should stay inside its experimental range (mean $\pm$ 2SD of 12 trials). As an example, the deviation index d_a was calculated as:

$$d_a = \frac{1}{n_a} \sum_{i=1}^{n_a} \sum_{k=0}^{2N} d_{a_{i,k}}, \tag{9}$$

with:

$$d_{a_{i,k}} = \begin{cases} \dfrac{q_{i,k} - \hat{q}_{i,k}^{(\mathrm{ub})}}{\hat{q}_{i,k}^{(\mathrm{ub})} - \hat{q}_{i,k}^{(\mathrm{lb})}}, & \text{if } \; q_{i,k} > \hat{q}_{i,k}^{(\mathrm{ub})} \\ \dfrac{\hat{q}_{i,k}^{(\mathrm{lb})} - q_{i,k}}{\hat{q}_{i,k}^{(\mathrm{ub})} - \hat{q}_{i,k}^{(\mathrm{lb})}}, & \text{if } \; q_{i,k} < \hat{q}_{i,k}^{(\mathrm{lb})} \\ 0, & \text{otherwise} \end{cases}, \tag{10}$$

where: n_a is the number of joint angles, N is the number of mesh intervals in a half gait cycle, $q_{i,k}$ is the i-th predicted joint angle at the k-th mesh point, while $\hat{q}_{i,k}^{(\mathrm{ub})}$ and $\hat{q}_{i,k}^{(\mathrm{lb})}$ are the corresponding experimental upper and lower values (mean $\pm$ 2SD), respectively.

It is worth recalling that while the lower-level multi-objective OCP expressed by Eqn. (8b) is solved to synthesize a gait (the one associated with given weights $\mathbf{w}$), the upper-level optimization in Eqn. (8a) identifies the optimal weights $\mathbf{w}^*$ by properly exploring the PO front defined by the control objectives. Weights $\mathbf{w}^*$ represent the contribution (if any) of each selected control objective to the hidden optimal control pol-

icy encoded in the nervous system for locomotion. From a computational standpoint, it is interesting to realize that the search space of the upper-level optimization problem is profitably restricted by the bound constraints $\mathbf{w} \in [\mathbf{0}, \mathbf{1}]$ and by the equality constraint in Eqn. (8c) (the latter reduces the effective number of unknown weights to $(m-1)$), to the benefit of computational efficiency.

The upper-level optimization problem (8) was solved by the `patternsearch` algorithm from MATLAB's Global Optimization Toolbox [44], a derivative-free direct-search method with a global scope: we selected this deterministic algorithm because our optimization problem may easily be affected by some level of non-smoothness, as is often the case with numerical noise deriving from the underlying discretization (which may cause approximation of derivatives by finite differences to be quite unreliable, see also [45]). Also, we preferred a deterministic method over evolutionary/genetic algorithms, stochastic in nature and computationally intensive. The generating set search `GSSPositiveBasis2N` was selected as mesh poll option, as it is particularly efficient when only linear constraints are present. To minimize the risk of getting trapped at a local minimum, the option `UseCompletePoll` was set to true. To maximize computational efficiency, the solution process was parallelized: we used the option `UseParallel` to call the upper-level objective function (Eqn. (8a)) and constraints (Eqns. (8b) and (8c)) in parallel using eight cores.

Selecting suitable stopping criteria for direct-search methods is not trivial (especially for evolutionary algorithms). In this case, however, a valid termination criterion can be easily established thanks to the described formulation of the upper-level problem. When `patternsearch` polls mesh points in the neighborhood of a solution, it gradually shrinks the mesh until its linear dimension (`MeshSize`) is less than a prescribed value (`MeshTolerance`). In the problem at hand, the mesh is naturally well scaled ($\mathbf{w} \in [\mathbf{0}, \mathbf{1}]$), thus it is straightforward to set `MeshTolerance` to a reasonable minimum significant variation in each weight w_i: we set it to 0.5%. This is also very helpful in containing the total number of function evaluations and iterations.

It is worth recalling that the lower-level OCP expressed by Eqn. (8b) is iteratively solved using the MATLAB implementation of the CasADi/IPOPT solver.

2.6 Simulation scenarios

The effectiveness of our framework was assessed by solving the following two bilevel optimization problems:

- *bilevel weighting*, where the lower level was formulated with the weighting method as per Eqn. (5)

- *bilevel weighted Chebyshev* (*bilevel Chebyshev* hereafter), where the lower level was formulated with the weighted Chebyshev metric as per Eqn. (8b).

To further minimize the risk of getting trapped by local minima, the weights were initialized with six different initial guesses spanning the entire search space of the upper level, and the best result (minimum deviation d) was selected.

The obtained results were compared with those from [4] (*manual weighting*), all cost functionals being equal. A *tracking* simulation was also performed to assess the ability of the NMS model to reproduce the experimental gait data. To this end, we solved an OCP where deviations of predicted joint angles, ground reaction forces, and joint torques from their experimental counterparts (from a reference trial) were minimized. Additional details can also be found in the supplementary material of [4].

3 RESULTS AND DISCUSSION

A single bilevel optimization problem was solved in four to nine hours (depending on the selected initial guess for weights) on an eight-core laptop (2.4 GHz processor, 32 GB RAM). On average, about 90 function evaluations (that is, 90 lower-level OCP solutions) were required.

Table 1 shows the identified optimal weights (listed in the same order as $J_1, \ldots, J_5$) and the deviation index d for all the simulation scenarios. Predicted trajectories are plotted in Fig. 6 and Fig. 7 against experimental data (mean $\pm$ 2SD) over a full gait cycle. Since symmetry conditions between right and left body sides were imposed in the OCP, trajectories are shown only for the right side, plus the pelvis and trunk. In Fig. 7, muscle activations and electromyographic (EMG) signals are normalized with respect to the peak activations predicted by the bilevel Chebyshev.

A first result to highlight is the fact that the tracking simulation yielded trajectories that strictly follow the experimental data, meaning that the adopted NMS model is suitable for the purpose of our research.

Second, as evident from Table 1 and Fig. 6, both bilevel scenarios significantly improved on the manual weighting method, with the bilevel Chebyshev outperforming the bilevel weighting. Although the deviation index from the bilevel Chebyshev is half that from the bilevel weighting, their predicted trajectories are quite

	OPTIMAL WEIGHTS	d
manual weighting [4]	$(2, 1000, 0.5, 50, 1) \times 10^3$	6.070
bilevel weighting	$(0.452, 0.011, 0.416, 0.088, 0.033)$	0.335
bilevel Chebyshev	$(0.237, 0.244, 0.354, 0.057, 0.108)$	0.163

Table 1. Optimal weights and deviation index

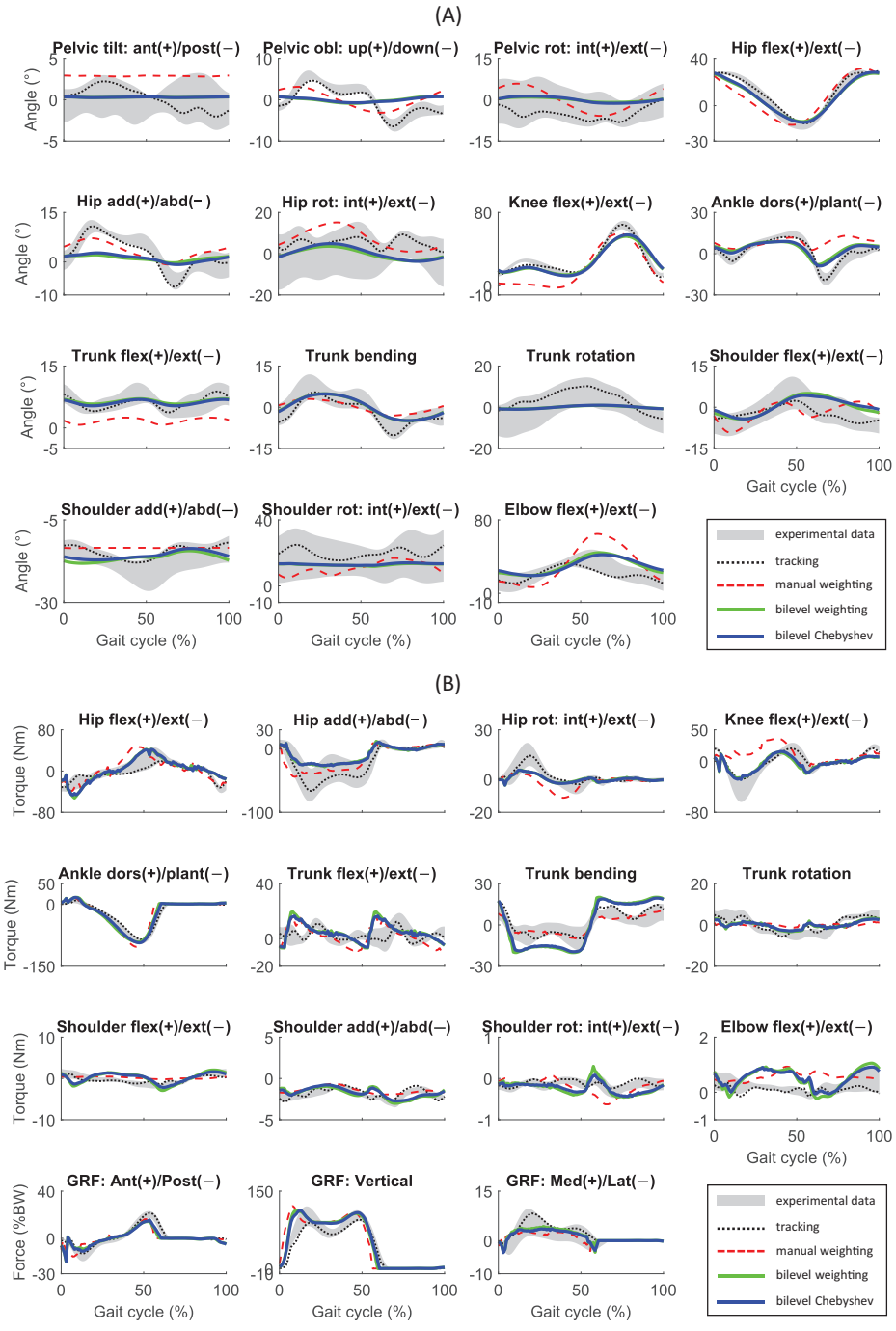

Fig. 6. Predicted (A) joint angles and (B) joint torques and ground reaction forces vs. experimental data

close to each other (Figs. 6 and 7). This is probably due to a limited extent of the PO front defined by the selected objectives. Furthermore, salient features of human locomotion are captured by both bilevel scenarios. Also predicted muscle activations (not included in the deviation index) (Fig. 7) are quite similar

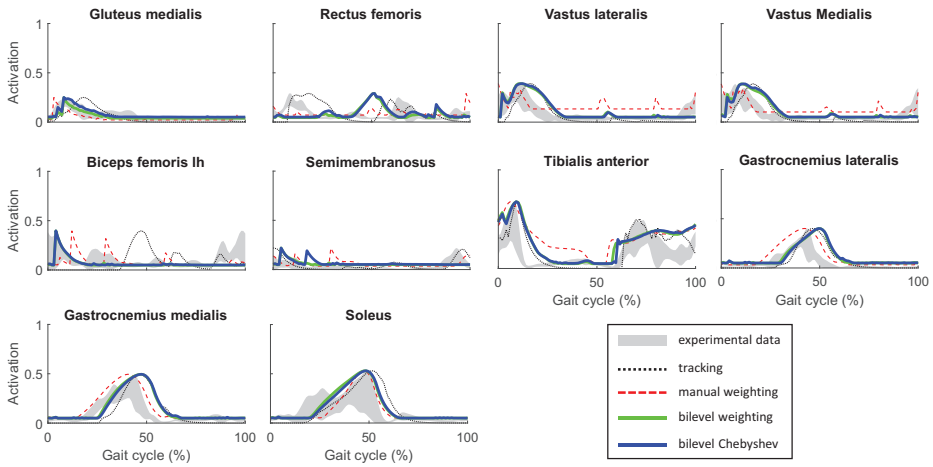

Fig. 7. Predicted muscle activations vs. experimental EMG signals

to their EMG signals.

Third, the optimal weights identified with the manual weighting and the bilevel weighting are not really interpretable for the reasons already discussed in the Methods section. Conversely, those obtained with the bilevel Chebyshev assume a more precise mathematical significance: penalizing metabolic energy rates ($w_3 \simeq 35\%$), muscle activations ($w_1 \simeq 24\%$), and arm excitations ($w_2 \simeq 24\%$) seems to play a major role in obtaining a human-like walking pattern than joint accelarations ($w_4 \simeq 6\%$) and passive joint torques ($w_5 \simeq 11\%$).

Nonetheless, some discrepancies between the variables predicted by the bilevel scenarios and their experimental counterparts should be emphasized. The peak in knee flexion at loading response is not fully captured, although bilevel simulations provided better results than the manual weighting. Also pelvic obliquity, and consequently hip adduction/abduction, are not well represented. As a consequence, reduced net torques are observable at the same joints. Ankle plantarflexion is rather limited at the push-off phase. The vertical component of the ground reaction forces increases more rapidly than the experimental one. The activation of the rectus femoris at loading response is not captured by any of the predictive scenarios, neither are the terminal-swing peaks in the vasti, biceps femoris and semimembranosus. Such findings suggest that the shock-absorption mechanisms at the hip and knee joints adopted by humans during locomotion are not well represented by the selected objective functionals. At the knee, quadriceps normally activate during the loading response to decelerate the rate of knee flexion induced by the heel rocker initiated by floor contact: thus, part of the knee joint load is transferred to the thigh muscles [46], and, as a consequence, the joint load is reduced (the impact with the floor is mitigated). At the hip, the abductor muscles normally restrain the rate of contralateral pelvic drop caused by the rapid loading of the stance limb (and rapid unloading of

the contralateral limb). Again, the impact associated with limb loading is "absorbed" by the muscular action and thus the total load experienced by the stance hip joint is reduced. The failure in capturing such shock-absorption mechanisms could explain why (i) the rectus femoris does not activate at loading response, and (ii) the vertical ground reaction force grows rapidly with respect to the experimental one. These observations suggest that a cost functional accounting for the knee and hip joint loads should be included.

It is important to highlight the limitations of the present study. Since predicted results strongly depend on the physical fidelity of the model on which simulations are based, the NMS model could be improved in terms of both DOFs and musculotendon actuators. By way of example, the knee joint could be integrated with rotations on the transverse and frontal planes, while a metatarsophalangeal joint could be added at the foot. In fact, the reduced ankle plantarflexion during push-off could also be explained by the absence of the metatarsophalangeal joint (as also pointed out in [47]). To further improve the model, novel techniques based, for instance, on shear wave propagation could be employed for the estimation of mechanical properties and loading of musculotendon units [48]. Another limitation of this study is that experimental motion capture data from a single, healthy subject were used. Even though multiple trials from the same subject were considered, a larger cohort of subjects with different anthropometric measures should be included to verify whether the same considerations still apply. The presence of local minima, typical of nonlinear optimization problems due to their nonconvexity, could also affect the validity of our findings. As opposed to global minima, local minima are the locally optimal solutions that most derivative-based optimization algorithms are designed to obtain. In the bilevel optimization framework presented here, the problem of local minima could affect both levels. At the lower level, it was addressed by initializing each OCP with the best available data-informed initial guess (obtained from multiple walking trials of the same subjects). However, suboptimal local minima may still be obtained. Global optimization algorithms could be employed instead of IPOPT, but massive parallelization would be required. The same concepts are valid for the upper level, where we tried to mitigate this problem by using settings for the `patternsearch` algorithm designed to make it more global in scope, and by initializing the problem with six different initial guesses. It should also be emphasized that reflex-driven control strategies, such as those by Geyer et al. [49], were not included in our work, but feedback integration could play a key role in situations where sensory noise and external disturbances are present. Finally, this study has been conducted using a deterministic approach, while probabilistic strategies could be devised to handle uncertainties connected with, for example, the parameters of the NMS model and/or noisy experimental data.

4 CONCLUSIONS

An inverse optimal control strategy to identify optimality criteria in human locomotion has been proposed in the form of a bilevel optimization framework. In the lower level, prediction of walking is formulated and solved as a multi-objective OCP based on a weighted Chebyshev metric, whereas the contributions of the selected cost functionals are systematically and efficiently identified in the upper level. The potential of our framework to predict features of human walking has been investigated, and all results have been compared to experimental data. Regarding the ability to reproduce the experimentally observed kinematic and kinetic trajectories, noteworthy improvements have been obtained with respect to recently published results. In addition, the special formulation of the proposed method has allowed valuable computational savings. However, some deviations from experimental data are still clearly observable, which may be caused by limitations in both the NMS model and the candidate motor control objectives. In particular, the typical shock-absorption mechanisms involving the hip and knee joints are not adequately captured, hence future research might benefit from including additional control objectives, such as penalizing hip and knee joint loads. The proposed framework is general enough to allow investigation of other motor tasks, as well as impaired movement, with the ultimate goal of learning the control objectives that best explain observed human motion.

ACKNOWLEDGEMENTS

The authors would like to express their gratitude to Dr. Antoine Falisse for the fruitful discussions and for his suggestions on how to adapt his computational framework for our investigations.

REFERENCES

[1] Bernstein, N., 1984, "The techniques of the study of movements," In *Human Motor Actions Bernstein Reassessed*, H. Whiting, ed., Vol. 17 of *Advances in Psychology*. North-Holland, pp. 1–26.

[2] Seth, A., and Pandy, M. G., 2007, "A neuromusculoskeletal tracking method for estimating individual muscle forces in human movement," *Journal of biomechanics,* **40**(2), pp. 356–366.

[3] Steele, K. M., DeMers, M. S., Schwartz, M. H., and Delp, S. L., 2012, "Compressive tibiofemoral force during crouch gait," *Gait & posture,* **35**(4), pp. 556–560.

[4] Falisse, A., Serrancolí, G., Dembia, C. L., Gillis, J., Jonkers, I., and De Groote, F., 2019, "Rapid predictive simulations with complex musculoskeletal models suggest that diverse healthy and patho-

logical human gaits can emerge from similar control strategies," *Journal of The Royal Society Interface,* **16**(157), p. 20190402.

[5] Dembia, C. L., Bianco, N. A., Falisse, A., Hicks, J. L., and Delp, S. L., 2019, "Opensim moco: Musculoskeletal optimal control," *BioRxiv*, p. 839381.

[6] Febrer-Nafría, M., Pallarès-López, R., Fregly, B. J., and Font-Llagunes, J. M., 2020, "Comparison of different optimal control formulations for generating dynamically consistent crutch walking simulations using a torque-driven model," *Mechanism and Machine Theory,* **154**, p. 104031.

[7] Nubar, Y., and Contini, R., 1961, "A minimal principle in biomechanics," *The Bulletin of Mathematical Biophysics,* **23**(4), pp. 377–391.

[8] Chow, C., and Jacobson, D., 1971, "Studies of human locomotion via optimal programming," *Mathematical Biosciences,* **10**(3-4), pp. 239–306.

[9] Ralston, H., 1976, "Energetics of human walking," In *Neural control of locomotion*. Springer, pp. 77–98.

[10] Todorov, E., 2004, "Optimality principles in sensorimotor control," *Nature Neuroscience,* **7**(9), pp. 907–915.

[11] Parker, G. A., and Smith, J. M., 1990, "Optimality theory in evolutionary biology," *Nature,* **348**, pp. 27–33.

[12] Febrer-Nafría, M., Pallarès-López, R., Fregly, B. J., and Font-Llagunes, J. M., 2020, "Prediction of three-dimensional crutch walking patterns using a torque-driven model," *Multibody System Dynamics,* **51**, pp. 1–19.

[13] Falisse, A., Pitto, L., Kainz, H., Hoang, H., Wesseling, M., Van Rossom, S., Papageorgiou, E., Bar-On, L., Hallemans, A., Desloovere, K., et al., 2020, "Physics-based simulations to predict the differential effects of motor control and musculoskeletal deficits on gait dysfunction in cerebral palsy: a retrospective case study," *Frontiers in Human Neuroscience,* **14**, p. 40.

[14] Tomasi, M., and Artoni, A., 2020, "Muscle contracture modeling and optimal control for crouch gait prediction," Vol. 9: 40th Computers and Information in Engineering Conference (CIE) of *ASME IDETC/CIE* V009T09A032.

[15] Handford, M. L., and Srinivasan, M., 2016, "Robotic lower limb prosthesis design through simultaneous computer optimizations of human and prosthesis costs," *Scientific Reports,* **6**, p. 19983.

[16] Millard, M., Sreenivasa, M., and Mombaur, K., 2017, "Predicting the motions and forces of wearable robotic systems using optimal control," *Frontiers in Robotics and AI,* **4**, p. 41.

[17] Zhou, L., Li, Y., and Bai, S., 2017, "A human-centered design optimization approach for robotic ex-

oskeletons through biomechanical simulation," *Robotics and Autonomous Systems,* **91**, pp. 337–347.

[18] Gidley, A. D., Marsh, A. P., and Umberger, B. R., 2019, "Performance criteria for generating predictive optimal control simulations of bicycle pedaling," *Computer Methods in Biomechanics and Biomedical Engineering,* **22**(1), pp. 11–20.

[19] Ackermann, M., and Van den Bogert, A. J., 2010, "Optimality principles for model-based prediction of human gait," *Journal of Biomechanics,* **43**(6), pp. 1055–1060.

[20] Lee, L.-F., and Umberger, B. R., 2016, "Generating optimal control simulations of musculoskeletal movement using OpenSim and MATLAB," *PeerJ,* **4**, p. e1638.

[21] Nguyen, V. Q., Johnson, R. T., Sup, F. C., and Umberger, B. R., 2019, "Bilevel optimization for cost function determination in dynamic simulation of human gait," *IEEE Transactions on Neural Systems and Rehabilitation Engineering,* **27**(7), pp. 1426–1435.

[22] Mombaur, K., and Clever, D., 2017, "Inverse optimal control as a tool to understand human movement," In *Geometric and Numerical Foundations of Movements*. Springer, pp. 163–186.

[23] Meyns, P., Bruijn, S. M., and Duysens, J., 2013, "The how and why of arm swing during human walking," *Gait & Posture,* **38**(4), pp. 555–562.

[24] Angelini, L., Di Puccio, F., Zander, T., and Schmidt, H., 2016, "Influence of arm motion on spatio-temporal gait parameters and on force data," *IOSR Journal of Sports and Physical Education,* **3**, pp. 12–17.

[25] Anderson, F. C., and Pandy, M. G., 2001, "Dynamic optimization of human walking," *J. Biomech. Eng.,* **123**(5), pp. 381–390.

[26] Selinger, J. C., O'Connor, S. M., Wong, J. D., and Donelan, J. M., 2015, "Humans can continuously optimize energetic cost during walking," *Current Biology,* **25**(18), pp. 2452–2456.

[27] Miller, R. H., 2014, "A comparison of muscle energy models for simulating human walking in three dimensions," *Journal of Biomechanics,* **47**(6), pp. 1373–1381.

[28] Long III, L. L., and Srinivasan, M., 2013, "Walking, running, and resting under time, distance, and average speed constraints: optimality of walk-run-rest mixtures," *Journal of The Royal Society Interface,* **10**(81), p. 20120980.

[29] Lin, Y.-C., Walter, J. P., and Pandy, M. G., 2018, "Predictive simulations of neuromuscular coordination and joint-contact loading in human gait," *Annals of Biomedical Engineering,* **46**(8), pp. 1216–1227.

[30] Miller, R. H., Umberger, B. R., Hamill, J., and Caldwell, G. E., 2012, "Evaluation of the minimum energy hypothesis and other potential optimality criteria for human running," *Proceedings of the Royal Society*

B: Biological Sciences, **279**(1733), pp. 1498–1505.

[31] Umberger, B. R., and Miller, R. H., 2018, "Optimal control modeling of human movement," *Handbook of Human Motion*, pp. 327–348.

[32] Clever, D., Hatz, K., and Mombaur, K., 2014, "Studying dynamical principles of human locomotion using inverse optimal control," *PAMM,* **14**(1), pp. 801–802.

[33] Clever, D., Hu, Y., and Mombaur, K., 2018, "Humanoid gait generation in complex environments based on template models and optimality principles learned from human beings," *The International Journal of Robotics Research,* **37**(10), pp. 1184–1204.

[34] Lin, J. F.-S., Carreno-Medrano, P., Parsapour, M., and Sakr, M., 2021, "Objective learning from human demonstrations," *Annual Reviews in Control,* **51**, pp. 111–129.

[35] Betts, J. T., 2010, *Practical Methods for Optimal Control and Estimation Using Nonlinear Programming, Second Edition* Society for Industrial and Applied Mathematics.

[36] Veerkamp, K., Waterval, N., Geijtenbeek, T., Carty, C., Lloyd, D., Harlaar, J., and van der Krogt, M., 2021, "Evaluating cost function criteria in predicting healthy gait," *Journal of Biomechanics,* **123**, p. 110530.

[37] Seth, A., Hicks, J. L., Uchida, T. K., Habib, A., Dembia, C. L., Dunne, J. J., Ong, C. F., DeMers, M. S., Rajagopal, A., Millard, M., Hamner, S. R., Arnold, E. M., Yong, J. R., Lakshmikanth, S. K., Sherman, M. A., Ku, J. P., and Delp, S. L., 2018, "OpenSim: Simulating musculoskeletal dynamics and neuromuscular control to study human and animal movement.," *PLoS Comput Biol,* **14**(7), p. e1006223.

[38] Thelen, D. G., 2003, "Adjustment of muscle mechanics model parameters to simulate dynamic contractions in older adults," *Journal of Biomechanical Engineering,* **125**(1), pp. 70–77.

[39] Andersson, J. A. E., Gillis, J., Horn, G., Rawlings, J. B., and Diehl, M., 2019, "CasADi – A software framework for nonlinear optimization and optimal control," *Mathematical Programming Computation,* **11**(1), pp. 1–36.

[40] Wächter, A., and Biegler, L. T., 2006, "On the implementation of an interior-point filter line-search algorithm for large-scale nonlinear programming," *Mathematical Programming,* **106**(1), pp. 25–57.

[41] Bhargava, L. J., Pandy, M. G., and Anderson, F. C., 2004, "A phenomenological model for estimating metabolic energy consumption in muscle contraction," *Journal of Biomechanics,* **37**(1), pp. 81–88.

[42] Miettinen, K., 1999, *Nonlinear multiobjective optimization* Kluwer Academic Publishers, Norwell, MA, USA.

[43] Bowman, V. J., 1976, "On the relationship of the Tchebycheff norm and the efficient frontier of multiple-

criteria objectives," In *Multiple Criteria Decision Making. Lecture Notes in Economics and Mathematical Systems (Operations Research)*, H. Thiriez and S. Zionts, eds., Vol. 130. Springer, Berlin, Heidelberg.

[44] MATLAB R2020a, 2020, Global Optimization Toolbox (version 4.3) The MathWorks, Natick, MA, USA.

[45] Artoni, A., 2019, "A methodology for simulation-based, multiobjective gear design optimization," *Mechanism and Machine Theory,* **133**, pp. 95–111.

[46] Perry, J., 1992, *Gait Analysis. Normal and Pathological Function* SLACK Incorporated.

[47] Falisse, A., Afschrift, M., and De Groote, F., 2022, "Modeling toes contributes to realistic stance knee mechanics in three-dimensional predictive simulations of walking," *PloS one,* **17**(1), p. e0256311.

[48] Blank, J. L., Thelen, D. G., Allen, M. S., and Roth, J. D., 2022, "Sensitivity of the shear wave speed-stress relationship to soft tissue material properties and fiber alignment," *Journal of the Mechanical Behavior of Biomedical Materials,* **125**, p. 104964.

[49] Song, S., and Geyer, H., 2015, "A neural circuitry that emphasizes spinal feedback generates diverse behaviours of human locomotion," *The Journal of physiology,* **593**(16), pp. 3493–3511.